Numerical simulation of magnetotelluric fields at Stromboli

A. Franke, S. Kütter, R.-U. Börner and K. Spitzer
TU Bergakademie Freiberg, Germany

1 Summary

Stromboli is a small volcanic island in the Mediterranean Sea off the west coast of Italy. It is famous for its characteristic Strombolian eruptions. To get a better understanding of these processes further explorations of the inner structure of the volcano are essential. By carrying out numerical simulations, we aim at showing that the magnetotelluric method using a wide frequency range, e.g. $10^{-4}...10^{4}$ Hz, is applicable to this task.

To compute accurate electromagnetic fields the geometry of Stromboli volcano and the surrounding bathymetry need to be considered as detailed as possible. This becomes feasible using 2D and 3D finite element techniques on unstructured triangular and tetrahedral grids. First numerical simulations of MT measurements are computed applying a generalized geometry: a frustum as the volcano, an underlying halfspace and a layer of sea water surrounding the volcano.

Keywords: magnetotellurics, volcano, numerical simulation

2 Introduction

Stromboli volcano is 926 m high and extends down beneath the sea level to a depth of 2000 m. The first activities of the Palaeostromboli took place during the younger Pleistocene about 40,000 years ago. The characteristic Strombolian eruptions have proceeded in approximately the same manner for at least the last two thousand years. To get a better understanding of the processes that lead to eruptions further investigations of the inner structure of the volcano are essential. As shown by Müller and Haack (2004) the magnetotelluric (MT) method might be applicable to this task. In order to calculate highly accurate results, a detailed description of the geometry of Stromboli volcano and the surrounding bathymetry is necessary. We apply 2D and 3D finite element techniques on unstructured triangular and tetrahedral grids to incorporate arbitrary surface and seafloor topography (Franke, Börner and Spitzer, 2007).

First numerical simulations of MT measurements are computed applying a generalized geometry: a frustum of 3000 m height as the volcano, an underlying halfspace with a thickness of 5000 m and a layer of sea water surrounding the volcano. The electromagnetic fields, apparent resistivities and phases are calculated numerically at the seafloor, the slopes, and on top of the volcano. To resolve the upper structure of the volcano including the chimney as well as the layers underneath the volcano and the magma chamber, the computations are carried out for a wide frequency range.

3 Magnetotelluric method

The behaviour of electromagnetic fields is governed by Maxwell's equations. Assuming a harmonic time dependency $e^{i\omega t}$ as well as the magnetic and electric fields $\mathbf{H}$ and $\mathbf{E}$ as

$$\mathbf{H} = \mu^{-1}(\nabla \times \mathbf{A}) \quad \text{and} \quad \mathbf{E} = -i\omega\mathbf{A} - \nabla V,$$

the equation of induction for the magnetic vector potential $\mathbf{A}$ reads

$$\nabla \times \mu^{-1}(\nabla \times \mathbf{A}) + (i\omega\sigma - \omega^2\varepsilon)\mathbf{A} \quad = \quad 0$$

where the electric scalar potential V has been eleminated by a gauge condition.

To solve the boundary value problem in the bounded domain Ω, electric and magnetic insulation are required for boundaries parallel ($\Gamma_{||}$) and perpendicular ($\Gamma_{\perp}$) to the current flow, respectively:

$$\mathbf{n} \times \mathbf{H} = 0 \quad \text{on} \quad \Gamma_{||} \qquad \text{and} \qquad \mathbf{n} \times \mathbf{A} = 0 \quad \text{on} \quad \Gamma_{\perp}.$$

Furthermore, the magnetic field values for the top and bottom boundaries are calculated analytically for a 1D layered halfspace:

$$H_{\perp} = 1\,\mathrm{Am}^{-1} \quad \text{on} \quad \Gamma_{top} \qquad \text{and} \qquad H_{\perp} = H(z) \quad \text{on} \quad \Gamma_{bottom}.$$

The conditions of continuity for the magnetic fields apply to at all interior boundaries representing possible jumps in the conductivity:

$$\mathbf{n}_1 \times \mathbf{H}_1 + \mathbf{n}_2 \times \mathbf{H}_2 \quad = \quad 0 \quad \text{on} \quad \Gamma_{int}.$$

To interpret MT measurements, apparent resistivity and phase are computed from the electromagnetic fields

$$\rho_{ij} = \frac{1}{\omega\mu} \mid Z_{ij} \mid^2, \quad \phi_{ij} = arg(Z_{ij}) \quad \text{with} \quad Z_{ij} = \frac{E_i}{H_j} \quad \text{and} \quad i,j = x,y$$

where Z_{ij} is the impedance for different directions of polarisation.

4 The model

The geometry of Stromboli volcano and the surrounding bathymetry have to be considered as detailed as possible to obtain results that are close to reality. First 2D simulations of MT measurements imply a generalized geometry depicted in fig. 1 with the following parameters: a frustum of 3 km height as the volcano, an underlying halfspace with a thickness of 100 km, a 2 km thick layer of sea water and an air layer of 100 km. The electrical conductivities are assigned according to Friedel and Jacobs (1997) and UNESCO (1983). Preliminary 3D calculations use an axially symmetric model (cf. fig. 2) with a 50 km×50 km×17 km sized rectangular prism surrounding the volcano.

To the 2D simulations, we apply the finite element method using unstructured triangular grids and quadratic Lagrange elements. In the 3D case, tetrahedral grids and quadratic Nèdèlec elements are employed to compute the electromagnetic fields. These approaches are very well suited to take into account the steep topography and bathymetry.

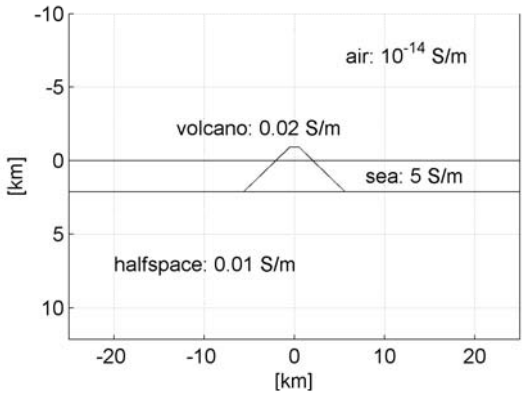

Fig. 1: Section of the 2D model including the electrical conductivity distribution.

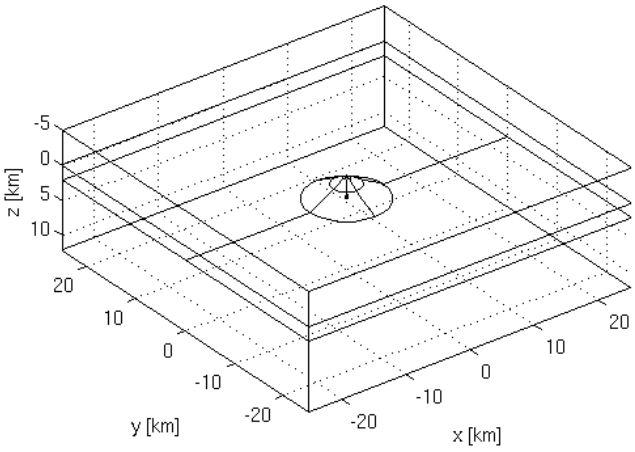

Fig. 2: 3D model.

5 Model studies

For the first analysis of the behaviour of MT data we have carried out 2D computations. Fig. 3 displays sounding curves of the apparent resistivity ρ_a and phase ϕ for the E-polarisation case on top of the volcano at $x = 0$ (left) and on the seafloor at $x = 50\,\mathrm{km}$ (right), respectively.

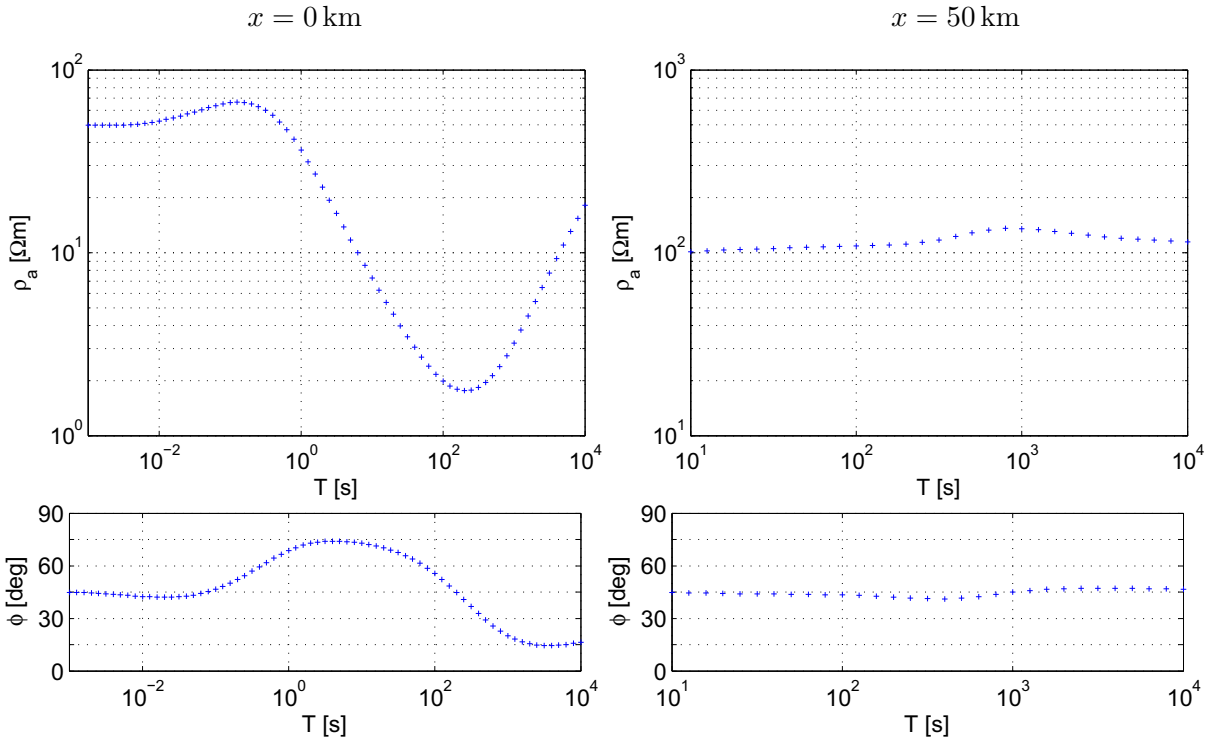

Fig. 3: 2D sounding curves of apparent resistivity (top) and phase (bottom) for E-polarisation on top of the volcano (left) and on the seafloor at $x = 50\,\mathrm{km}$ (right).

On the seafloor, the effect of the volcano i.e. the deviations from the halfspace resistivity of $100\,\Omega\,\mathrm{m}$ and phase of $45\,^\circ$ are small and limited to the period range of $10^2...10^4\,\mathrm{s}$ (cf. fig. 3, right). These periods yield a skin depth that is larger than the thickness of the sea layer and they are suited to register a lateral effect of the resistive volcano. On

top of the volcano, however, as shown in fig. 3 (left) the apparent resistivity and phase show variations for periods between 10^{-2} and 10^4 s due to the conductive sea water and the underlying halfspace. Hence, the challenge is to simulate the electromagnetic fields for a wide frequency range that is suited to yield information about the conductivity distribution of the halfspace and the volcano itself.

For the H-polarisation case, sounding curves of apparent resistivity ρ_a and phase ϕ on top of the volcano $x = 0$ and on the seafloor $x = 300\,\mathrm{km}$ are depicted in fig. 4. On top of the volcano, the data show a strong static shift effect for periods longer than 10 s (cf. fig. 4, left). Due to the charge accumulation at the high conductivity contrast between the volcano and the highly conductive sea water the electric field on top of the volcano increases and, hence, yields higher apparent resistivities. The phase is not affected by the in-phase oscillating charge accumulation.

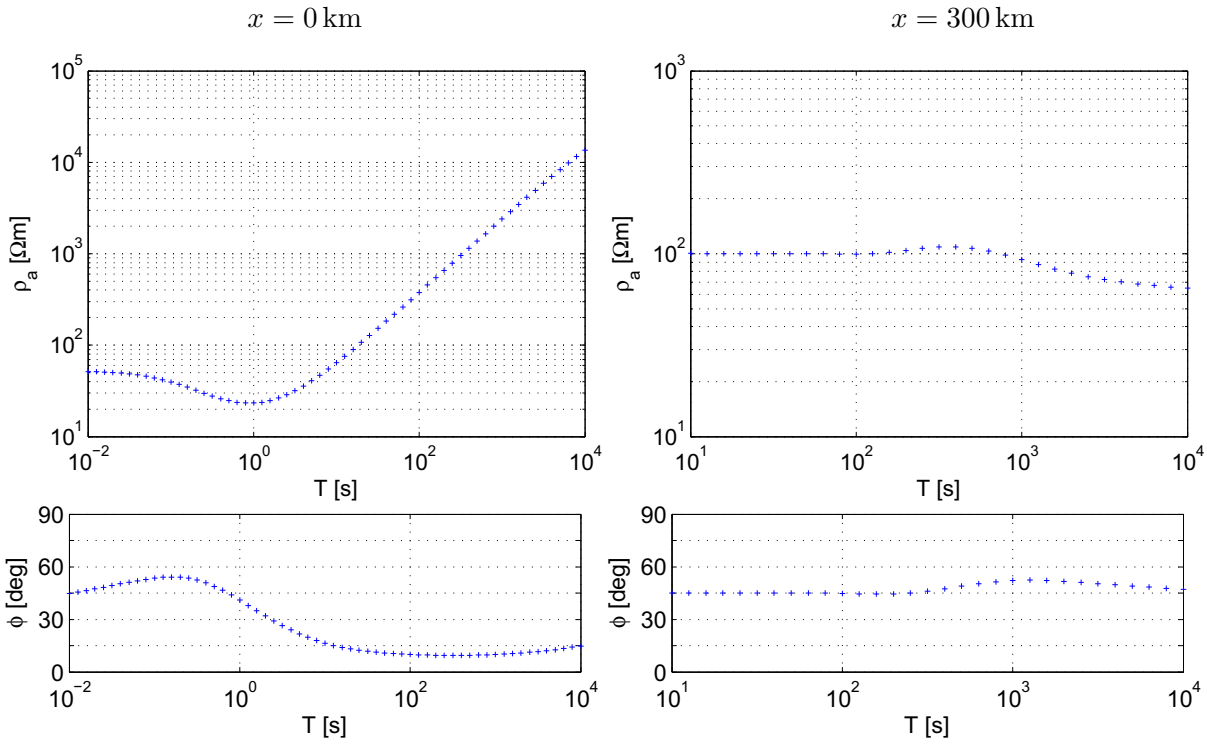

Fig. 4: 2D sounding curves of apparent resistivity (top) and phase (bottom) for H-polarisation on top of the volcano (left) and on the seafloor at x=300km (right).

The 3D simulations show a very complex behaviour of the apparent resistivity and the phase. Since we do not have any analytical solution for the volcano model to compare with and convergency studies are not feasible because the 3D computations are still very time consuming and memory demanding we invoke the symmetry of the model to validate our simulation results. Fig. 5 displays the location of the data points 1 to 5 with respect to the midpoint of the bottom face of the frustum representing the volcano that is situated in the origin of the coordinate system. Considering xy-polarisation, i.e. H_y is the incident field, the appropriate electric field component E_x is parallel to the profile for the data points 4 and 5, however, it is perpendicular to the profile for the data points 2 and 3. By contrast, in the yx-polarisation case, i.e. considering H_x as the incident field, the electric field component E_y is parallel to the profile for the data points 1 and 2 but it is perpendicular to the profile for the data points 4 and 5. Since the model is axially symmetric regarding the z-axis, we expect the same results e.g. for ρ_{xy} at data point 2 and ρ_{yx} at point 4 ($E_\perp$, 10 km, cf. fig. 6, left). Similarly, congruent sounding curves e.g. for ρ_{yx} at point 3 and ρ_{xy} at point 5 ($E_{||}$, 15 km) are shown in fig 7 and in fig. 8 for data point 1. As expected, beside small errors due to the numerical approach the sounding curves are congruent for symmetry reasons.

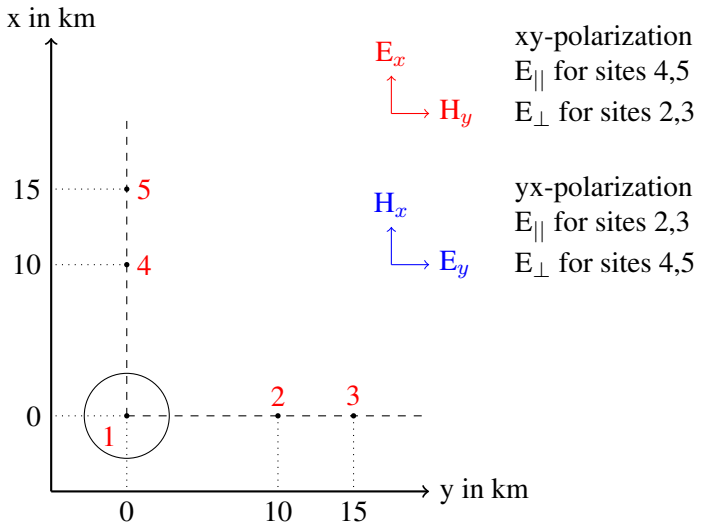

Fig. 5: Experimental design

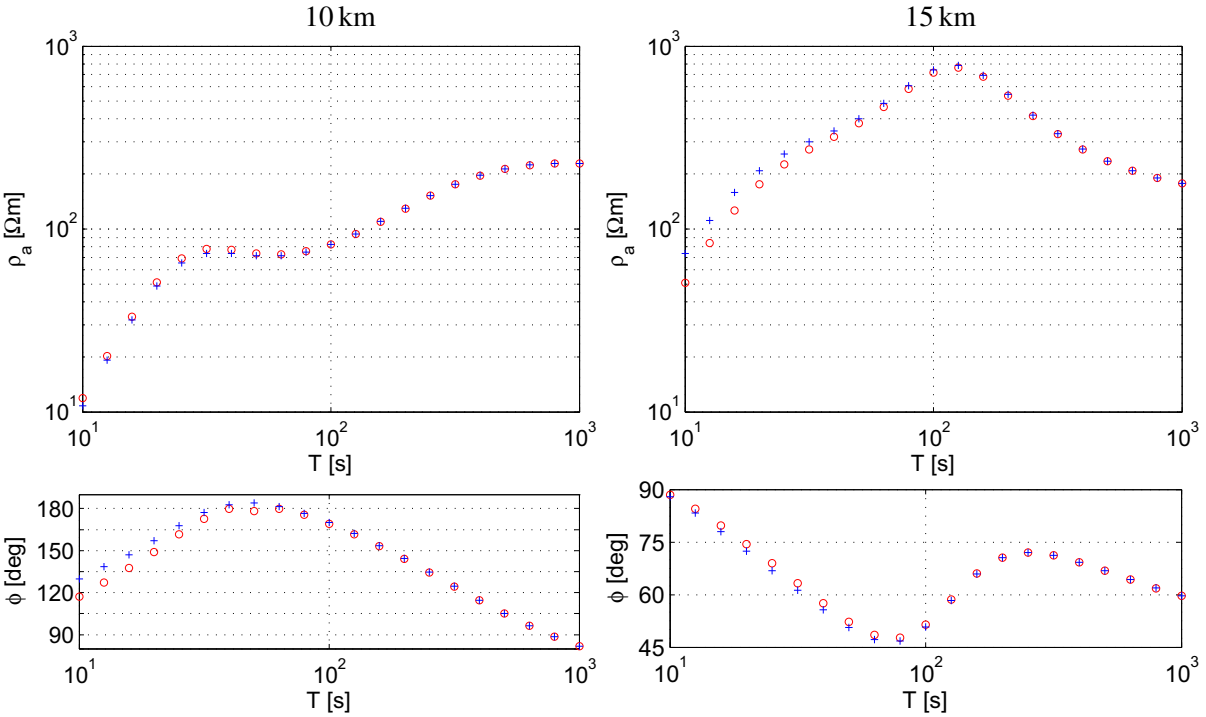

Fig. 6: Sounding curves of apparent resistivity ρ_a (top) and phase ϕ (bottom) at a distance of 10 km at data points 2 '○' and 4 '+' (left) and 15 km at data points 3 '○' and 5 '+' (right) for $E_\perp$, '○' xy-polarization, '+' yx-polarization

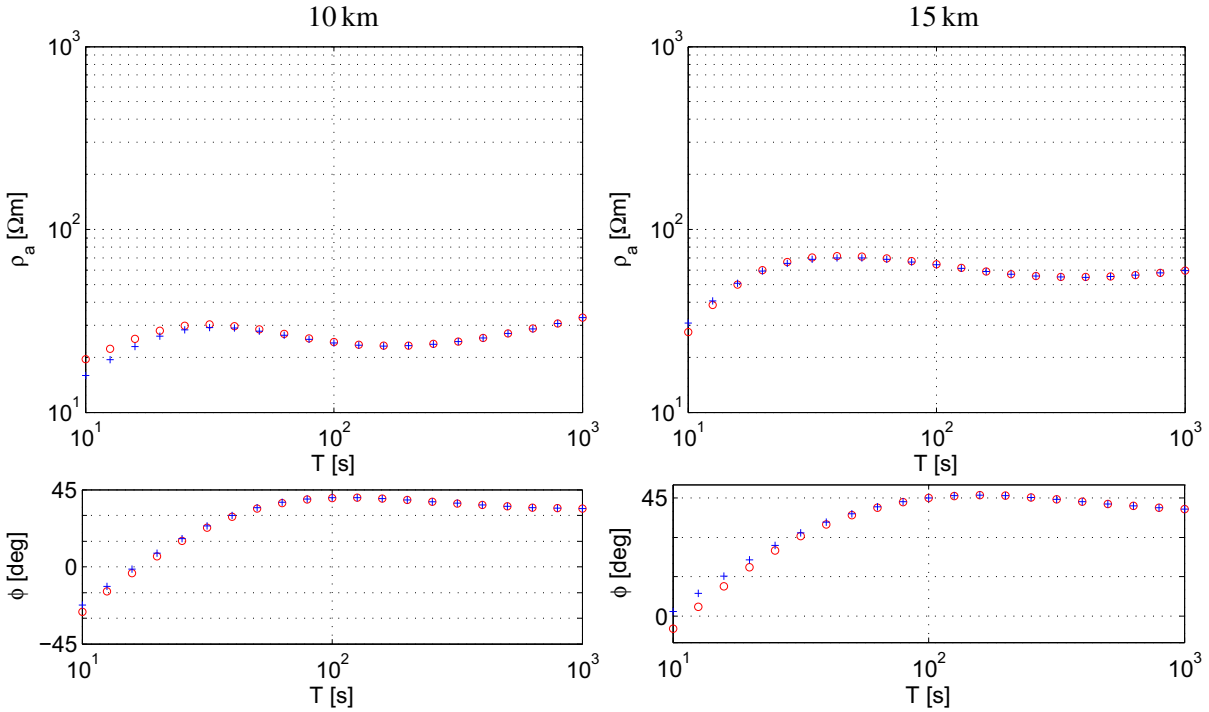

Fig. 7: Sounding curves of apparent resistivity ρ_a (top) and phase ϕ (bottom) at a distance of 10 km at data points 4 '○' and 2 '+' (left) and 15 km at data points 5 '○' and 3 '+' (right) for $E_{||}$, '○' xy-polarization, '+' yx-polarization

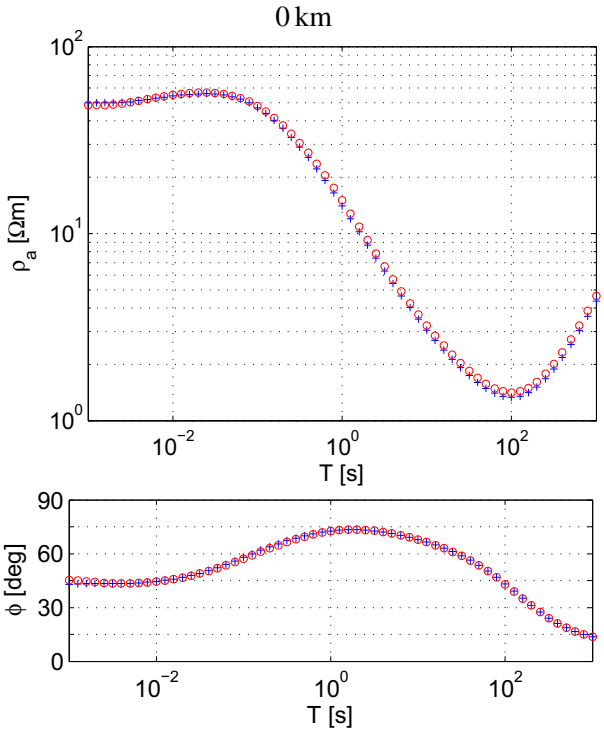

Fig. 8: Sounding curves of apparent resistivity ρ_a (top) and phase ϕ (bottom) on top of the volcano at data point 1 (x=0 km), ○ xy-polarization, + yx-polarization

6 Conclusions

We have presented our first promising results for simulating MT data at volcano Stromboli. In order to provide detailed information about the interior structure of the volcano that is of great interest with regard to eruption processes the elctromagnetic fields need to be computed for a wide frequency range and interpreted on the volcano as well as on the seafloor. We have applied the finite element method using unstructured triangular and tetrahedral grids that are well suited to take into account the topographic and bathymetric effects of the volcano's slopes. By examining the distribution of the current density and the electromagnetic fields themselves a more fundamental understanding of the underlying physical phenomena might be achieved. In the future, more detailed model studies aim at resolving rising gas bubbles associated with Strombolian eruption processes. Furthermore, to be even closer to reality we intend to use real topography and bathymetry data of Stromboli in the form of digital elevation models.

References

Franke, A., Börner, R.-U. and Spitzer, K. (2007). Adaptive unstructured grid finite element simulation of two-dimensional electromagnetic fields for arbitrary surface and seafloor topography. *Geophysical Journal International*, *in press*.

Friedel, S. and Jacobs, F. (1997). *DFG-Arbeitsbericht (Ja 590/6-1): Geoelektrische Untersuchungen zur Erforschung des strukturellen Aufbaus sowie von vulkanischen Aktivitäten und Vorläuferphänomenen am Dekadenvulkan Merapi* (Tech. Rep.).

Müller, A. and Haack, V. (2004). 3-D modeling of the deep electrical conductivity of Merapi volcano (Central Java): Integrating magnetotellurics, induction vectors and the effects of steep topgraphy. *Journal of volcanology and geothermal research*, *138*, 205-222.

UNESCO. (1983). Algorithms for computation of fundamental properties of seawater. *Unesco Techn. Pap. in Mar. Sci.*, *44*.